Effect of pH and pH-shifting on Lignin, Lignin-protein Properties, and Lignin-protein Interactions

Sarocha Pradyawong
Kansas State University
Ruben Shrestha
Kansas State University
Ping Li
Kansas State University
Xiuzhi Susan Sun
Kansas State University
Donghai Wang (dwang@k-state.edu)
Kansas State University https://orcid.org/0000-0001-9293-1387

Research Article

Keywords: Lignin, Protein, Interactions, pH, pH-shifting, Adhesive

Posted Date: July 16th, 2021

DOI: https://doi.org/10.21203/rs.3.rs-696743/v1

Abstract

Innovation of high-value added lignin derivatives has become a topic of interest, but lignin modification and utilization remain a challenge due to lignin's complicated structure. In our previous study, we successfully improved water resistance and adhesion performance of soy protein adhesives using unmodified lignin. This study focuses on lignin modification as well as lignin-protein properties and interactions. Lignin modification was achieved by pH changes and pH-shifting. Cleavage of β-O-4 linkage was observed at pH 8.5 and pH 12, resulting in smaller particle sizes and changes in thermal properties. Partial repolymerization was found after pH-shifting treatments. Lignin increased the strength of protein films under high temperature and significantly enhanced the water resistance of soy protein at pH 12. Cross-linking of protein and lignin took place via carbonyl, amino, and hydroxyl groups. Multiple-point interactions between lignin and protein resulted in a stronger lignin-protein network. Additional lignin-protein complexes with high molecular weight were detected with an elevated lignin concentration at pH 8.5. The binding interaction between lignin and protein, although of non-specific nature, was also observed by isothermal titration calorimetry (ITC). Findings of this study contribute to the further development of green lignin-protein products.

1. Introduction

Lignin accounts for 30% of the carbon source on earth.[1, 2] It is largely available as a renewable, amorphous, aromatic bio-polymer. As a sustainable source of monomers, lignin has drawn significant interest in the last few decades as a potential building block for bio-based products and materials.[3, 4] Lignin, modified lignin, and its derivatives are good fillers and property enhancers for both petroleum- and bio-based materials.[1, 5, 6] Recent green research has also examined the use of lignin in such diverse products as polymers, plastics, and adhesives.[4, 7–14] Although many studies have confirmed lignin's potential as an alternative aromatic source, very little lignin is currently utilized as high value-added products.[15] Most of the lignin by-products from paper, plumping, and biomass industries are flamed to generate heat in factories.[16, 17] Given lignin's sustainability and availability, along with the environmental concerns and the crisis caused by our dependence on fossil fuels, there is an urgent demand for more thorough studies on lignin and innovations in lignin applications.[10]

Lignin is polyelectrolyte in an aqueous solution. It can be depolymerized and modified to smaller phenolic compounds. The phenolic group can easily form hydrogen bond (H-bond) with the carboxylic group of protein.[18] Cross-linking interactions between polyphenol and protein have been reported.[19–21] Polyphenols can form multiple interactions and cross-links with peptide chains at more than one point.[22] The cross-linked networks are strengthened by hydrophobic and hydrophilic binding and Van der Waals forces. These interactions change proteins' physicochemical properties, for example, lowering their solubility and increasing thermal stability.[18] Similar interactions between lignin/lignin derivatives and protein have also been reported. Reversible interactions such as hydrogen bonding, hydrophobic and electrostatic force, and non-specific interactions also occur in the lignin-protein adsorption process.[23] In

addition, cross-coupling interactions are formed between 3 types of polar amino acids and coniferyl alcohol, the major subunit of lignin.[2]

However, the mechanism of lignin-protein interactions is still poorly understood,[18] and understanding this mechanism is a key step to improving the properties of bio-based adhesives and films. A few research groups have reported the application of lignin as a wet strength enhancer for soy protein-based adhesives; however, very little supporting information of lignin-protein interaction has been provided. Moreover, morphological changes in protein caused by lignin interaction. Therefore, the objectives of this research were 1) to prove the interactions between lignin and protein at different pH values and with pH shifting and 2) to observe the morphological changes of protein caused by lignin-protein interactions.

2. Materials And Methods

2.1 Sample Preparation

ALDRICH alkali lignin (No. 370959) (AL) was purchased from Sigma-Aldrich, Inc. (St. Louis, MO) and dispersed in distilled water (DW) to reach the concentration of 10% (w/w). Sodium hydroxide (NaOH) and hydrochloric acid (HCl) were supplied by Fisher Scientific (Fair Lawn, NJ) and used as received to adjust the pH of lignin solutions. For non-pH-shifting lignin samples, pH was adjusted to 4.5, 8.5, and 12 and maintained for 24 hr. The samples were labeled L4.5, L8.5, and L12, respectively. For pH-shifting lignin samples, pH was first maintained at 8.5 and 12 for 24 hr and then adjusted to 4.5 and kept constant for 2 hr. These samples were labeled L8.5-4.5 and L12.5-4.5. Fresh lignin samples were used later to prepare adhesives. Portions of the samples were dried at 150°C for 10 minutes for further analysis. The experiment was conducted under high temperature in order to understand the lignin-protein interactions and properties due to the effects of the hot-press process using in wood industries.

Defatted soy flour (Cargill, Cedar Rapids, IA) with 90 dispersion index was obtained as a protein source. Protein extraction was conducted at 6.5% solid content in DW. pH of the slurry was adjusted with NaOH (10N) to 8.5 to solubilize protein. Protein precipitation then took place at pH 4.2 by HCl (10N). Protein parts were collected by centrifugation at 12,000 g. Protein chunks were collected and neutralized with NaOH (10N). Isolated soy protein (SP) was then freeze-dried, ground with a cyclone miller with a 1 mm screen (Udy Corp., Fort Collins, CO), and stored at 4°C. For non-pH-shifting SP, 10 percent of SP was dissolved in DW, and the pH was adjusted to 4.5, 8.5, and 12 by 3N HCl and NaOH and stirred for 2 hr. The samples were labeled SP4.5, SP8.5, and SP12, respectively. To make non-pH-shifting lignin-protein mixed adhesives, L4.5, L8.5, L12 fresh samples were added to SP4.5, SP8.5, and SP12, respectively. The adhesives were labeled SPL4.5, SPL-8.5, and SPL12. All samples were stirred at 300 rpm for 2 hr at room temperature. For pH-shifting SP, the pH of SP8.5 and SP12 was adjusted to 4.5 and kept constant for another 2 hr. The samples were labeled SP8.5-4.5 and SP12-4.5. For pH-shifting LSP, L4.5, L8.5, L12 were mixed with corresponding SP4.5, SP8.5, and SP12, respectively, and then stirred for 2 hr before shifting pH to 4.5 and holding for another 2 hr. The samples were labeled LSP8.5-4.5 and LSP12-4.5. Portions of

the samples were dried at 150°C for 10 minutes, ground by a hand grinder (CoorseTek 60311 Ceramic, Coli-Parmer, IL), and passed through a 100-mesh screen.

2.2 Characterization of Lignin Properties

Dried lignin samples from Sect. 2.1 were coated with palladium and gold by a sputter coater (Desk II Sputter/Etch Unit, Moorestown, NJ) and observed under a scanning electron microscope (SEM) (Hitachi S-3500N, Hitachi Science System, Ibaraki, Japan) for morphological changes. Images were collected at an accelerating voltage of 10.0 kV. The quantum mechanical magnetic properties of the samples were analyzed using the 2D-HSQC NMR technique. Approximately 40 mg of control, the purchased alkali lignin, and dried lignin samples from Sect. 2.1 were dissolved in 0.5 mL of dimethyl sulfoxide (DMSO). Spectra were measured by a 500 MHz Bruker AVIII spectrometer equipped with a cryogenically-cooled carbon observe probe. Spectral widths were 8012 and 20883 Hz for the ^{1}H and ^{13}C dimensions, respectively. The number of collected complex points for the ^{1}H dimension was 1024 with a recycle delay of 2 s. The number of transients was 2, and 256 time increments were recorded in the ^{13}C dimension. The $^{1}J_{C-H}$ used was 145 Hz. Data matrices were zero filled to 1024 points in the ^{13}C dimension. Data were processed by standard Bruker Topspin-NMR software. For thermostability analysis, approximately 5 mg of samples was heated from 25°C to 700°C. The heating rate was set to 10°C/min, and the inert atmosphere in the chamber was control by N_2. A thermogravimetric analyzer (Perkin-Elmer TGA 7, Norwalk, CT) was used to analyze the thermostability of dried lignin samples.

2.3 Evaluation of Morphological Properties

The particle sizes of lignin, SP, and SPL fresh samples from Sect. 2.1 were measured by a laser scattering particle size distribution analyzer, LA-910 (Hiroba Scientific, NJ). Fresh adhesives were then diluted to 0.1% with DW. The slurries were negatively stained with 2% aqua uranyl acetate and examined at 80.0 kV under a transmission electron microscope (TEM), TecnaiTM G2 Spirit BioTWIN (FEI Co., Hillsboro, OR). Fresh SP and LSP adhesives were used to prepare adhesive films on a premium micro slide plain (Fisherfinest, USA), and the film was oven dried at 150°C for 10 minutes. Photos of dried films were taken with a Samsung Galaxy S7 (Samsung, Korea). Morphology of the films was observed under an optical microscope (Olympus BX51, Olympus Corporation, Tokyo, Japan) with 45° reflection of fluorescent light. Dried films were soaked under DW for 2 hr. Underwater films were again captured with the Samsung Galaxy S7 (Samsung, Korea). The morphologies and characteristics of the films were studied.

2.4 Analysis of Lignin-Protein Interactions

SDS-PAGE was run on 12% separation gel and 4% stacking gel in a discontinuous buffer system as previously described (G Qi et. al., 2011) to study protein and lignin-protein network molecular weight distribution. The samples (20 mg/ml) were mixed with loading buffer containing 2.1% SDS, 26.3% glycerol, 0.01% bromophenol blue, and 5% mercaptoethanol at pH 6.8 at a ratio of 1:1. SDS-PAGE was carried out under the reducing condition. After boiling for 5 minutes, 10 µl of the mixture was loaded into wells. Electrophoresis was conducted under 150 V and 40 mA for 90 min. The molecular weight standard (10–250 kDa) (Precision Plus Protein™ Standards, Dual color, BIO-RAD, CA) was loaded with the mixture.

The gel was then stained with 0.25% Coomassie brilliant blue R- 250 and destained in a destaining solution containing 30% acetic acid, 30% methanol, and 40% distilled deionized water. The binding interaction between lignin and soy protein was studied using isothermal titration calorimetry (ITC) (MicroCal iTC_{200}, GE Healthcare). L8.5 and SP8.5 were diluted to the concentrations of 84 and 3 µM, respectively. The diluted L8.5 was injected into the diluted SP8.5 in 19 injections of 2 µL (5 s), with an injection interval of 180 s, a reference power of 8 µcal/s, and a stirring speed of 750 rpm. Cell temperature was set at 25°C. In the control experiment, lignin was injected into buffer alone. Thermograms were evaluated using Origin (version 7, OriginLab), and data sets were fitted to the “one set of sites” model. The elemental compositions of lignin, protein, and lignin protein samples were measured using the CHNS/O Elemental Analyzer (PerkinElmer 2400 Series II, PerkinElmer Inc., Waltham, MA). Two to 2.5 mg of the dried samples from Sect. 2.1 was weighed by a PerkinElmer AD-6 Autobalance (PerkinElmer Inc., Waltham, MA) and packed with foil. The samples were then burned in a pure oxygen atmosphere in a combustion chamber. The gaseous products from combustion (CO_2, N_2, SO_2, and H_2O) were separated and detected in a quartz column by a thermoconductometer detector. PerkinElmer SpectrumTM 400 FTIR/FT-NIR spectrophotometer (Shelton, CT) was used to scan the spectra of the dried samples. Fourier transform infrared (FTIR) data were collected in the range of 500–4000 cm^{-1}. The transmission spectra of 32 scans were collected at a resolution of 4 cm^{-1}.

3. Result And Discussion

3.1 Lignin Properties

2D-HSQC analysis is a powerful method to determine lignin structures.[24] $^{13}C^{1}H$ correlation spectra in the 2D-HSQC analysis of the lignin samples were identified according to previous literatures.[24-26] The side-chain region (δ_C/δ_H 50.0–90.0/2.50–6.00) and aromatic region (δ_C/δ_H 100.0–150.0/5.50–8.50) of lignin are shown in Fig. 1A-1F and 1a-1f, respectively.

According to Fig. 1A, the original kraft lignin (control) showed prominent C-H correlations of β-O-4 linkages at C_α-H_α (δ_C/δ_H 71.3/4.76ppm), C_β-H_β (δ_C/δ_H 83.9/4.30ppm), and C_γ-H_γ (δ_C/δ_H 60.2/3.35-3.69ppm). A strong signal of methyl groups was observed at δ_C/δ_H 55.7/3.77 ppm. The presence of resinol (Fig. 3II) was confirmed by C-H correlations of C_α-H_α, C_β-H_β, and C_γ-H_γ at δ_C/δ_H 85.3/4.62, 53.7/3.04, and 71.0/3.76 and 4.16 ppm, respectively. The major component of the kraft lignin is G subunits, as dense signals at δ_C/δ_H 109.6/7.16, 115.4/6.74, and 119.6/6.97 ppm represent C_2-H_2, C_5-H_5, and C_6-H_6 of guaiacyl units (G), respectively (Fig. 1a). The light spot at δ_C/δ_H 103.5/6.63 of $C_{2,6}$-$H_{2,6}$ implies a low amount of S units in the kraft lignin. Correlations from $C_{2,6}$-$H_{2,6}$ in the p-hydroxyphenol structure were observed at δ_C/δ_H 128.2/7.17 ppm.

Acidic pH at 4.5 had a minor influence on lignin structure since similar spectra were observed between the control and L4.5. On the other hand, alkaline environment caused significant changes in lignin structure. A decrease in correlation intensity of the methoxyl groups (δ_C/δ_H 55.7/3.77 ppm) was observed in all

alkali treated lignins. The C-H correlations of C_{α}-H_{α} and C_{β}-H_{β} of β-o-4 linkages disappeared, and a low response of C_{γ}-H_{γ} in L8.5, L12, and L12-4.5 indicated the cleavage of β-O-4 linkages, which resulted in higher phenolic hydroxyl groups.[27] Some β-O-4 linkages were reformed after pH shifting in alkali treatment (i.e., L8.5-4.5); however, this was not observed when the initial pH was extremely high (i.e., L12-4.5). A similar scenario was found in β-β linkage in resinol (Fig. 3II). The signal assigned to S units was invisible in all pH-treated lignin samples. The C-H correlations of p-hydroxyphenol (*) also disappeared in alkali and alkali-shifting treatments. Compared with untreated lignin, alkali treated lignin samples have a less intense C_5-H_5 signal and only a faint response at C_2-H_2, and C_6-H_6 positions. These findings confirm the replacement of H atoms in C_2, C_6, and C_5 of G units.

Changes in lignin structure obtained from NMR were confirmed by morphological images. Unmodified lignin was scanned at 400x magnification as seen in Fig. 2a. A mixture of large particles, both rough and smooth, was observed, and the particles were separate from each other. Based on the NMR spectra, there was no significant change between L4.5 (Fig. 1B and b) and the control (Fig. 1A and a). But based on scanning electron images, L4.5 was depolymerized and contained smaller particles (Fig. 2b). These particles formed interactions and attached to each other as shown in Fig. 2b, indicating significantly smaller particle sizes and changes in electrostatic charges. On the other hand, alkaline treatments resulted in sharp-edged lignin as shown in Fig. 2c. Higher ratios of sharp-edged lignin were observed at the extremely high pH (Fig. 2e). Since acid hydrolysis broke down lignin into small particles, whereas base hydrolysis created sharp-edged lignin, the pH-shifting process accordingly created a mixture of both lignin characteristics (Fig. 2d and 2f). In addition, small linkages between 2 clamping particles were observed (Fig. 2d and 2f at the red arrows), which suggests additional lignin-lignin interactions and/or repolymerization after pH shifting.

Lignin is stable at high temperatures due to its condensed aromatic and highly branched structures. Thermal degradation of lignin occurs in a broad range of temperatures (Fig. 3) because lignin contains various aromatic side chains and branches attached to different positions on the aromatic units. The initial weight loss (25-200 °C) is mainly from moisture evaporation.[28] After that, pyrolysis reaction takes place and contributes to major weight loss. The first degradation stage is the dehydration of hydroxyl groups (150-275 °C) and breakage of ether bonds (150-300 °C). Then aromatic rings start to lose aliphatic side chains. Still higher temperatures (370-400 °C) break C-C linkage. After that, backbone degradation at temperatures between 500-700 °C results in gaseous products.[29] The degradation temperature is affected by fragmentation of inter-unit linkages and the content of C-C bonds.[30, 31] Lignin with higher degradation temperatures contains a higher portion of high molecular weight compounds.[32]

The thermal stability of unmodified lignin was slightly higher due to its high G content.[33] T_g of all modified lignins were in the range of 338.48-389.15 °C, whereas unmodified lignin T_g was 404.19 °C (Table 1), which suggests that acid, base, and pH shifting depolymerized lignin and resulted in lower molecular weight compounds. In Fig. 3, different derivative weight curve patterns suggested that different

subunits were produced in different treatments. Acid modification caused a lower T_g but did not significantly change the thermal profile of unmodified lignin. On the other hand, a shoulder around 410-430 °C appeared in L8.5 and both pH-shifting samples, suggesting repolymerization of lignin. L12 presented a distinctive thermoresistance profile: the first peak indicating water evaporation and hydroxyl group dehydration was bigger than that of other lignins. L12 also showed a unique weight loss profile (Table 1). More than a quarter of total weight loss came from the dehydration of hydroxyl groups and evaporation, whereas only 3-8 % of those was released in other modified lignins. This indicates that extremely high pH treatment increased lignin's hydroxyl groups and water binding capacity. Moreover, in L12, only about 55% of weight was lost between 200-500 °C, whereas 74-81% was lost in this range in other lignins. This suggests that in L12, some part of the lignin skeleton had broken in the extremely high pH environment, and some small compounds were released. These compounds likely contributed to the odor perceived during the sample preparation. As a result, a relatively small backbone degradation peak was observed in L12, and approximately 60% ash was recovered after the test. All lignins emitted approximately the same amount of gaseous products after 500 °C. L12 showed the highest thermoresistance properties with ~60% residual after 700 °C, indicating that lignins modified with a high pH are likely to be more thermostable than acid treated or untreated lignins.

3.2 Lignin-SP and SP Morphology

According to Fig. 4a, the average single agglomeration of pure SP was 60-70 nm. Larger agglomerations (less than 500 nm) also formed. Lignin linked protein agglomerations and resulted in a large clamp (Fig. 4b). The size of the lignin-protein network was larger than 500 nm. The quantitative analysis of particle sizes was shown in Table 2. Lignin particles became smaller and more uniformed after being treated with different pH values. In severe alkaline environment (pH 12), particles were undetectable, as all samples were completely soluble. Exposing protein to alkaline conditions before aggregation resulted in bigger clusters. The biggest cluster (131.559±32.526 μm) was observed after exposing protein to denaturing pH. This means that denatured protein can refold to looser structures that are different from the folding structures of non-denaturing protein.

The particle size of LSP8.5 was larger and more varied than that of SP8.5 and L8.5. The bigger complex may be caused by covalent bonds and cross-links between lignin and protein. Since the average particle size of LSP8.5 was bigger than the single-pair binding of L8.5-L8.5, L8.5-SP8.5, or SP8.5-SP8.5, multiple-interactions and lignin-protein networks could have formed. This suggests the existence of multiple active sides in lignin and protein and supports a model proposed in a previous study[7]. However, lignin-protein clusters at the isoelectric point of LSP4.5, LSP8.5-4.5, and LSP12-4.5 were smaller than that of SP4.5, SP8.5-4.5, and SP12-4.5, respectively. Since the active sites of protein already bonded to lignin, less active sites were available to form interactions with protein when the pH was brought to pI (pH 4.5). Moreover, the presence of lignin in the system disturbed the formation of large protein networks. As a result, the cluster of LSP was smaller than that of SP samples in all conditions.

Dried film morphology was shown in Fig. 5. At higher pH values, SP films turned yellow. LSP films also turned dark brown due to the brown color of lignin. All pH 4.5 and pH-shifting films were flat and had tendency to stick on the micro slide. At pH 8.5, film partially lifted from the slide and formed a corrugated film with air inside. Small bubbles were spread along the film in both SP and LSP samples. In contrast, a large bubble was formed in the middle of the SP12 film with cracks around (Fig. 5d), which suggests more cohesion at high pH values. Light reflection was seen in both SP12 and LSP12 dried films.

Film texture was observed under an optical microscope. More cracks were found in SP samples than LSP samples. Small bubbles, both broken and complete, were found in SP8.5, whereas in the LSP8.5 film, air was trapped and formed bigger unbroken bubbles (Fig.5 B and G). This indicates a stronger cohesion force in LSP films than in SP films. The higher strength of LSP films was also observed at pH 12: in the SP12 film, small fragments sprang from the main film at the edge of the bubble, whereas fragments were not observed in the LSP12 film (Fig.5 D and I). Therefore, lignin strengthened and improved the cohesiveness of SP films.

Film morphology under water strongly reflects a sample's water resistance. The appearance of SP and LSP 4.5 were similar (Fig. 6a and f), while differences were observed in alkaline conditions. At pH 8.5, many small SP8.5 film pellets detached at the edge of the film, whereas the LSP8.5 film was intact with no free pellets (Fig. 6b and g). Conformational changes start to occur at pH values above 11,[34] and conformational changes and chemical changes influence each other. As protein denatured and unfolded, polar and non-polar groups were exposed and became more available to interact with lignin.[35] Thus, more remarkable improvement and protein-lignin interactions were detected at extreme alkaline pH values. The SP12 film floated freely and was completely dissolved (Fig. 6d). By contrast, the floated LSP12 film was thick and partially dissolved in water. The film absorbed water and formed a gelatinous pellet. The improvement in morphology after soaking in water demonstrates that lignin improves protein water resistance possibly by crosslinking and other lignin-protein interactions. As seen in Fig. 6c and h, mild pH shifting process (8.5-4.5) did not change the film appearance of SP and LSP samples. However, extreme alkali-shifting (12-4.5) affected protein solubility and led to the exposure of hydrophobic groups and cleavage of native S-S bonds.[36] With the interference of lignin on protein aggregation as mentioned in section 3.2, the LSP12-4.5 film showed many fractures, but the SP12-4.5 film stayed intact (Fig. 6e and j). Therefore, the water resistance of SP and SPL films is not only influenced by protein characteristics but also the strength of lignin-protein interactions as a consequence of pH and pH shifting.

3.3 Lignin-Protein Interactions

The syringe contained 84 μM lignin and the cell contained 3 μM soy protein. The 1st peak is a mock injection. Upper panel: raw data showing heat pulses obtained by multiple injections; Lower panel: integrated heat of binding as a function of molar ratio of ligand:macromolecule. The graph shown is after the subtraction of negative control where lignin was injected into the buffer.

The binding interaction of soy protein with lignin was studied using isothermal titration calorimetry (ITC). The exothermic peaks observed during the titration (Fig. 7) suggested that some binding took place. However, attempts to obtain reproducible 'N' values were unsuccessful, which led us to believe that the binding was of non-specific types. The interpretation of binding was further complicated by the lack of specific molecular weight data for the lignin and soy protein. Hence, for the current observation, the molecular weight was estimated to be the sum total of molecular weights of all the subunits.

The differences between SP and LSP samples mentioned in sections 3.1 and 3.2 were found at pH 8.5. No band was detected in the negative control lignin sample (Fig. 8a, lane 1). In the pure SP sample (lane 2a), the distribution pattern of α0, α, and β subunits from 7S around 75 and 50 kD was similar to that found in Qi et al. (2011). Acid and basic polypeptides of 11S also appeared at lower molecular weight bands. The variation in molecular sizes could be caused by differences in electrostatic interactions at different pH values.[37] A similar protein subunit distribution pattern was presented in the LSP sample (Fig. 8a, lane 3), indicating that some polypeptides did not interact with lignin. A significant band was detected in LSP8.5 (lane 3a) around 250 kD and >250kD but not in SP8.5 (lane 2a), suggesting that lignin-protein complex was formed. As discussed in section 3.1, the lignin-protein networks were formed with a broad range of particle sizes, which correspond with the extensive bands (ranging from ~30 to >250 kD). This phenomena was also reported in a previous study in which high molecular weight fractions of cross-coupling products, coniferyl alcohol (a lignin major subunit)-amino acids complex, were observed.[2] Lignin-protein complex fractions were also observed at room temperature. The same protein subunit distribution pattern was also found in fresh SP and LSP samples. There were no bands in lignin samples (Fig. 8b lane 1). The lignin-protein complex band was found in the same size range as in Fig. 8a, and the band intensity elevated from Fig. 8b lane 3 to lane 7 as lignin concentration increased from 10 to 50%, indicating that more lignin-protein complexes were formed with more lignin in the system.

Elemental composition analysis reflects the overall composition of samples. Table 3 shows (%) the ratio of oxygen to carbon atoms (O/C) of lignin, protein, and lignin-protein samples. The O/C of the lignin was 35.21% at pH 4.5. The (%) O/C increased to 84.51 and 75.28 for L12 and L12-4.5, respectively. The additional oxygen atom in the structure mainly resulted from the cleavage of β-O-4, which created more active groups such as hydroxyl group. This is especially the case in extreme alkali environments. These data confirmed the 2D-HSQC NMR results in section 3.1 that more reactions and changes occurred in extremer alkali treatments.

The (%) O/C of protein was consistent in SP4.5, SP8.5, and SP8.5-4.5. The higher (%) O/C was found at denaturing pH (pH 12). This may be caused by hydrolysis of the peptide bond (-CO-NH-) on the polypeptide chain, which resulted in –COOH and -NH_2 groups. The additional oxygen atom in –COOH group could have contributed to the significantly higher (%) O/C in SP12 and SP12-4.5. The changes in LSP samples followed the same pattern.

The (%) O/C of Lignin+SP was calculated based on the blending ratio of lignin and SP with the assumption that there were no chemical and bonding interactions between lignin and protein that could change the compositions of the molecules. The difference between the actual value obtained from LSP samples and the calculated Lignin+SP value (Table 3) indicates changes in the oxygen content after reactions. The negative differences indicate an interaction between lignin and SP, since LSP samples have less oxygen than the calculated Lignin+SP values. Loss of oxygen could imply covalent crosslink interactions between lignin and protein samples. Since lignin and protein have active groups such as amino, hydroxyl, carbonyl, and carboxyl groups, the reactions that involved oxygen were likely to be condensation and esterification.

At the most extreme condition of pH 12-4.5, lignin, soy protein, and lignin-soy protein gave the clearest IR spectra. The IR spectrum of lignin shows aromatic skeleton vibrations at 1595, 1510, and 1422 cm^{-1}. The shoulder at 1701 cm^{-1} corresponds to the C=O stretching in conjugated carbonyl compounds with aromatic rings. The absorption at 1457 is attributed to C-H bending and vibrations of aromatic groups. The absorption peak at 1213 and 1029 corresponds to C-O bond and bending vibrations of G subunit's aromatic plane, respectively.[38]

Protein major absorption bands Amide I, II, and III were observed at 1640, 1520, and 1233, respectively. Amide I contains major stretching vibrations of the amide group (80%) and C-N bond. Amide II peak comes from N-H bending (60%) and C-N stretching (40%) vibrations. Amide III peak mainly describes C-N stretching vibrations and N-H in-plane bending vibrations.

According to Fig 9, compared to SP samples, LSP samples showed differences in all 3 amide peaks. First, the amide I absorption peak of LSP was slightly weaker than that of SP. This indicates the stronger H-bond near the C=O group. The stronger H-bond reduces electron density around C=O and results in a lower absorption intensity. In an extreme pH environment, extended peptide chains are aligned closer to neighboring chains after unfolding, which contributes to strong intermolecular hydrogen bonds. Second, the amide II peak absorption of LSP showed a slight shift in peak shape and position. This could be caused by the influence of the lignin adsorption band or changes in the chemical environment, because frequency shifts can be true shifts or caused by relative intensities of component band variations. [39] The frequency and absorption bands of amide I and II could be influenced by the strength of hydrogen bonds involving amide C=O and N-H groups. The stronger H-bonds indicate stronger secondary structures in LSP samples. Last, the amide III peak of LSP was broader, and the peak slightly shifted from 1233 to 1230 cm^{-1} with the shoulder appearing at 1273 cm^{-1}. This change is possibly caused by the lignin absorption peak at the same position, 1273 cm^{-1}. However, it is difficult to interpret the amide III absorption band as it could also be influenced by C=O in-plane bending, C-C stretching, and CH_2 wagging vibrations. The absorption band at 1392 cm^{-1} is attributed to the stretching and vibration of the COO^- group.[40, 41] Since SP and LSP samples have the same-size absorption peak at 1447 cm^{-1}, while the LSP sample showed a relatively low 1392 cm^{-1} peak, it is highly possible that there were interactions between lignin and the COO^- group of protein. In addition, different absorption patterns between SP and

LSP samples were observed between 1200 and 1000 cm^{-1}. As the spectrum in the 1300-1000 cm^{-1} region is related to the C-O stretching of alcohol, phenol, and carboxylic groups, changes in the LSP sample might be caused by the influence of lignin absorption, interactions of C-O, changes in the chemical environment, or a combination of these factors.

Fig. 9b is the difference spectrum where the spectrum of SP is subtracted from that of LSP and compared with the spectrum of lignin. Additional peaks at 1728 and 1642 cm^{-1} represent stretching vibration of unconjugated and conjugated carbonyl groups (C=O), respectively.[38, 42-44] Fig. 9c is the difference spectrum where the spectrum of lignin is subtracted from that of LSP and compared with the spectrum of SP. In Fig. 9c, the amide I peak shifted to higher frequency together with an increase in peak intensity. A conjugated carbonyl group represented inter- and intramolecular hydrogen bonds that generally occur between O-H and N-H, for example, the $-COO^-$ and -OH groups of protein and lignin.[45] Thus, these changes in both subtracted LSPs spectra in Fig. 9b and c indicate that strong molecular interactions were formed between lignin and the C=O group of protein. An ester bond was possibly formed by alcoholysis and ammonolysis of -COOH in acid condition. Ester, ether, and the bonds between C/N, C/S, S/S were previously observed between amino acid side chains such as lysine and phenolic rings, and disulfide bonds between lignin and protein.[2, 18, 46], [47] Moreover, change in aromatic skeleton vibration was also observed. First, the 1595 cm^{-1} peak indicated a mixed signal of aromatic skeleton vibration and C=O stretching. The reference lignin peak response was from aromatic skeleton vibration, whereas the subtracted LSP peak response was from both aromatic skeleton vibration and C=O stretching. The peak intensity of subtracted LSP was less than that of the referenced lignin, indicating that lower response came from aromatic skeleton vibration. Second, the spectrum at 1510 cm^{-1} corresponds directly to the aromatic skeleton vibration, which disappeared after subtraction. Third, the amide II absorption band shifted from 1520 to the higher wavenumber 1540 cm^{-1}, and the relative intensity of amide II increased compared to that of amide I in the subtracted spectrum (Fig. 9c). These changes indicate a new C-N bond formation between protein and lignin.[48] The interaction between amino groups attached directly to C_2 and C_5 of phenolic compounds through quinine intermediate[18] limits molecular movement and vibration of the aromatic ring.

On the other hand, compared to the reference lignin spectrum, the subtracted LSP spectrum showed slightly shifted and stronger signals of C-O-C (1366), C-O of the G subunit (1273), C-C and C-O (1213), C-H in plane deformation (1143), C-O deformation of secondary alcohol and aliphatic ethers (1092), C-O of the guaiacyl group, and blending vibrations inside of the aromatic plane of the guaiacyl ring (1029). Stronger intensity in the range of 1000-1400 cm^{-1} indicated the formation of lignin-protein linkages. New absorption peaks at 1481, 900, and 836 cm^{-1} of the subtracted spectrum were observed. The new peaks likely indicate special covalent crosslinking between lignin and protein. However, further investigation is needed for more specific evidence. The changes in peak intensity in this range are likely caused by non-specific interactions. Strong cross-links are supported by many kinds of electrostatic interactions. H-bonds were claimed to be the dominant electrostatic interactions between protein and phenolic compounds in aqueous solutions[49] Hydrophobic interactions and electrostatic forces were also

observed between hydrophobic regions of soy protein and close to the rings of lignin. In addition, when lignin and protein molecules are close to each other, attraction and repulsion between positive and negative regions take place and lead to ion-dipole and ion-induced-dipole interactions and dipole-dipole interactions.[23] However, the mechanism of lignin-protein interactions has not been clearly elucidated.

It is difficult to predict or quantify lignin-protein interactions and networks because the formation of bonds and forces depends highly on the nature of lignin and protein and environmental factors. Lignin has different structures, functional groups, and molecular weights depending on plant species and extraction methods. In addition, various kinds of plant protein also have diverse amino acid sequences, subunit profiles, and folding structures. The diverse nature and structure of lignin and protein significantly determine the nature of interactions.[50] Reaction type and rate also highly depend on environmental conditions[45, 50, 51] Organic solvents and pH not only impact protein but also lignin, affecting their solubility, degree of folding, denaturing stage, exposure of functional groups, hydrophobic/hydrophilic properties, and degree of depolymerization.

4. Conclusion

In this study, lignin greatly improved protein adhesive properties, especially water resistance through the interactions between smaller lignin derivatives and unfolded/denatured protein structures. Lignin can be depolymerized in alkaline environments and partially repolymerized via the shifting to a lower pH. Lignin is capable of cross-linking and forming non-specific interactions with protein, resulting in higher molecular weight compounds that can be stabilized through chemical and heat treatments. Protein-lignin interactions occurred mainly between oxygen and nitrogen-related functional groups such as $-COO^-$ and –OH but also included non-specific interactions.

The use of lignin in bio-based applications remains a challenge because lignin's structures and functional groups depend highly on delignification processes and plant species. Lignin structure is complicated, consisting of various subunits and internal linkages, which make it difficult to study and uniform derivatives are also difficult to obtain. Moreover, lignin-protein interactions, network strength, morphology, and other properties are strongly influenced by modification methods and reaction conditions. Further study is required to clarify lignin-protein interactions in order to effectively utilize lignin as bio-based products for high-value-added applications.

Declarations

Conflicts of interest

There are no conflicts to declare.

Acknowledgements

Contribution number 20-278-J from the Kansas Agricultural Experiment Station

References

1. Pye EK (2008) Biorefineries-industrial processes and products: status quo and future directions: 165–200
2. Cong F, Diehl BG, Hill JL, Brown NR, Tien M (2013) Phytochemistry 96:449–456
3. Duval A, Lawoko M (2014) Reactive Functional Polymers 85:78–96
4. Huang J, Zhang L, Chen F (2003) J Appl Polym Sci 88:3284–3290
5. Lora JH, Glasser WG (2002) J Polym Environ 10:39–48
6. Holladay JE, White JF, Bozell JJ, Johnson D (2007) Pacific Northwest National Lab.(PNNL), Richland, WA (United States); National Renewable Energy Laboratory (NREL), Golden, CO (United States)
7. Pradyawong S, Qi G, Li N, Sun XS, Wang D (2017) International Journal of Adhesion and Adhesives
8. Luo J, Luo J, Yuan C et al (2015) RSC Advances 5:100849–100855
9. Ibrahim V, Mamo G, Gustafsson P-J, Hatti-Kaul R (2013) Ind Crops Prod 45:343–348
10. Wei M, Fan L, Huang J, Chen Y (2006) Macromol Mater Eng 291:524–530
11. Chen P, Zhang L, Peng S, Liao B (2006) J Appl Polym Sci 101:334–341
12. Huang J, Zhang L, Chen P (2003) J Appl Polym Sci 88:3291–3297
13. Zhang J, Chen Y, Sewell P, Brook MA (2015) Green Chem 17:1811–1819
14. Frigerio P, Zoia L, Orlandi M, Hanel T, Castellani L (2014) BioResources 9:1387–1400
15. El Mansouri N-E, Salvadó J (2006) Ind Crops Prod 24:8–16
16. Stewart D (2008) Ind Crops Prod 27:202–207. Doi:https://doi.org/10.1016/j.indcrop.2007.07.008
17. Mankar S, Chaudhari A, Soni I (2012) International Journal of Knowledge Engineering, ISSN: 0976–5816
18. Ozdal T, Capanoglu E, Altay F (2013) Food Res Int 51:954–970
19. Prodpran T, Benjakul S, Phatcharat S (2012) Int J Biol Macromol 51:774–782
20. Haslam E (1996) Journal of natural products 59:205–215
21. Damodaran S (2008) Amino acids, peptides, and proteins. CRC Press, Boca Raton
22. Mulaudzi R, Ndhlala A, Kulkarni M, Van Staden J (2012) J Ethnopharmacol 143:185–193
23. Salas C, Rojas OJ, Lucia LA, Hubbe MA, Genzer J (2012) ACS applied materials & interfaces 5: 199–206
24. Yang S, Yuan TQ, Li MF, Sun RC (2015) Int J Biol Macromol 72:54–62. Doi:10.1016/j.ijbiomac.2014.07.048
25. Yuan T-Q, Sun S-N, Xu F, Sun R-C (2011) J Agric Food Chem 59:10604–10614
26. Pu Y, Chen F, Ziebell A, Davison BH, Ragauskas AJ (2009) BioEnergy Research 2:198
27. Kuo M, Hse C-Y (1991) Holzforschung-International Journal of the Biology. Chemistry Physics Technology of Wood 45:47–54
28. Cao J, Xiao G, Xu X, Shen D, Jin B (2013) Fuel Process Technol 106:41–47

29. Laurichesse S, Avérous L (2014) Prog Polym Sci 39:1266–1290
30. Ibrahim MNM, Zakaria N, Sipaut CS, Sulaiman O, Hashim R (2011) Carbohyd Polym 86:112–119
31. Kim J-Y, Oh S, Hwang H, Kim U-J, Choi JW (2013) Polym Degrad Stab 98:1671–1678
32. Wen J-L, Sun S-L, Xue B-L, Sun R-C (2013) J Agric Food Chem 61:635–645
33. Wang S, Wang K, Liu Q et al (2009) Biotechnol Adv 27:562–567
34. Ishino K, Okamoto S (1975) Cereal chemistry
35. Hettiarachchy N, Kalapathy U, Myers D (1995) Journal of the American Oil Chemists' Society 72:1461–1464
36. Jiang J, Xiong YL, Chen J (2010) J Agric Food Chem 58:8035–8042
37. Qi G, Venkateshan K, Mo X, Zhang L, Sun XS (2011) J Agric Food Chem 59:9958–9964
38. Ibrahim MM, Nadiah MN, Azian H (2006) Journal of Applied Sciences 6:292–296
39. Stuart BH (2004) Infrared Spectroscopy: Fundamentals and Applications. John Wiley & Sons, Incorporated, Hoboken
40. Luo J, Luo J, Li X, Gao Q, Li J (2016) Journal of applied polymer science 133
41. Luo J, Li X, Zhang H, Gao Q, Li J (2016) Int J Adhes Adhes 71:99–104
42. Lisperguer J, Nunez C, Perez-Guerrero P (2013) J Chil Chem Soc 58:1937–1940
43. Singh SK, Ekhe JD (2014) RSC Advances 4:27971–27978
44. Poletto M, Zattera AJ (2013) Materials Research 16:1065–1070
45. Simon C, Barathieu K, Laguerre M et al (2003) Biochemistry 42:10385–10395
46. Fraenkel-Conrat H, Olcott HS (1945) J Biol Chem 161:259–268
47. Le Bourvellec C, Renard C (2012) Critical reviews in food science nutrition 52:213–248
48. Liu H (2017) Kansas State University
49. Hagerman AE, Butler LG (1981) J Biol Chem 256:4494–4497
50. Hagerman AE, Rice ME, Ritchard NT (1998) J Agric Food Chem 46:2590–2595
51. Zhang Y-J, Tanaka T, Betsumiya Y et al (2002) Chemical pharmaceutical bulletin 50:258–262

Tables

Table 1 Glass transition temperature (T_g) and weight loss (%) of lignin treated with different pH values and pH-shifting processes

Lignin	T_g(°C)	Wt. Loss/Total wt. loss (%)			Total loss (%)	Wt. remain (%)
		25-200 (C°)	200-500 (C°)	500-700 (C°)		
AL	404.19	7.05	76.13	16.81	57.15	42.85
L4.5	389.15	3.3	80.51	16.19	57.81	42.19
L8.5	338.48	7.52	74.33	18.15	46.58	53.42
L8.5-4.5	365.05	5.32	79.1	15.58	52.36	47.64
L12	379.71	26.49	54.72	18.78	39.13	60.87
L12-4.5	338.96	8.01	75.53	16.47	41.02	58.98

Table 2 Average particle size distribution of lignin, SP, and LSP treated with different pH values and pH-shifting processes

pH	Particle Size (μm)								
	Lignin			SP			LSP		
4.5	5.914	±	4.571	24.974	±	17.776	10.104	±	6.734
7	8.424	±	16.063		-			-	
8.5	4.800	±	3.815	7.550	±	1.906	32.650	±	42.886
8.5-4.5	2.785	±	1.164	29.519	±	18.670	17.832	±	11.413
12		-			-			-	
12-4.5	7.137	±	3.791	131.559	±	92.526	40.186	±	113.019

Table 3 Percentage of oxygen to carbon ratio (O/C*) of lignin, protein, and lignin-protein samples

	O/C*				
pH	Lignin	SP	Lignin+SP**	LSP	**Difference (%)*** **
4.5	35.21±0.12	47.22±0.04	45.21±0.06	45.42±0.20	**0.45±0.33**
8.5	38.54±1.50	48.21±2.17	46.60±2.06	44.96±0.54	**-3.46±3.10**
8.5-4.5	41.11±0.08	48.98±0.36	47.66±0.28	45.84±0.47	**-3.84±0.41**
12	84.51±0.86	58.68±0.07	62.99±0.20	59.09±1.17	**-6.19±2.16**
12-4.5	75.28±0.21	62.94±2.34	65.00±1.99	57.73±.044	**-11.16±2.04**

* $(\%)\ O/C = \frac{O(\%)/16}{C(\%)/12} x\ 100$

** Lignin+SP = (([%O/C_{lignin} x 0.2] + [%O/C_{SP} x 0.2])/1.2)x100

** Difference = (%O/C_{LSP} - %O/$C_{Lignin+SP}$) /%O/C_{LSP})x100

Figures

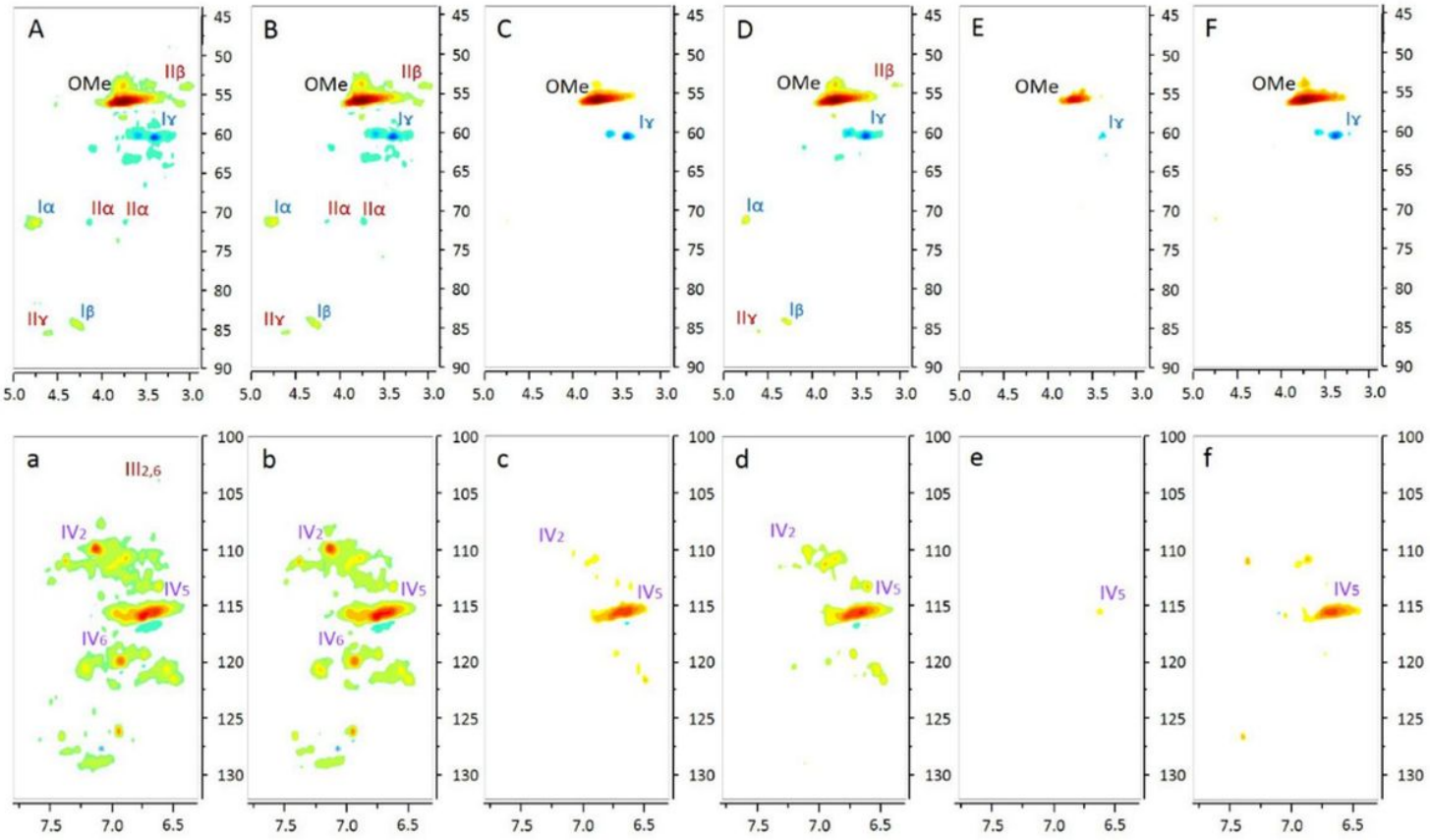

Figure 1

2D-HSQC-NMR spectra of lignin obtained at various pH values. (A, a) kraft lignin control; (B, b) L4.5; (C, c) L8.5; (D, d) L-8.5-4.5; (E, e) L12; (F, f) L12-4.5. Main structures in kraft lignin control: (I) β-O-4 ether linkage, (II) resinol, (III) syringyl units, and (IV) guaiacyl units.

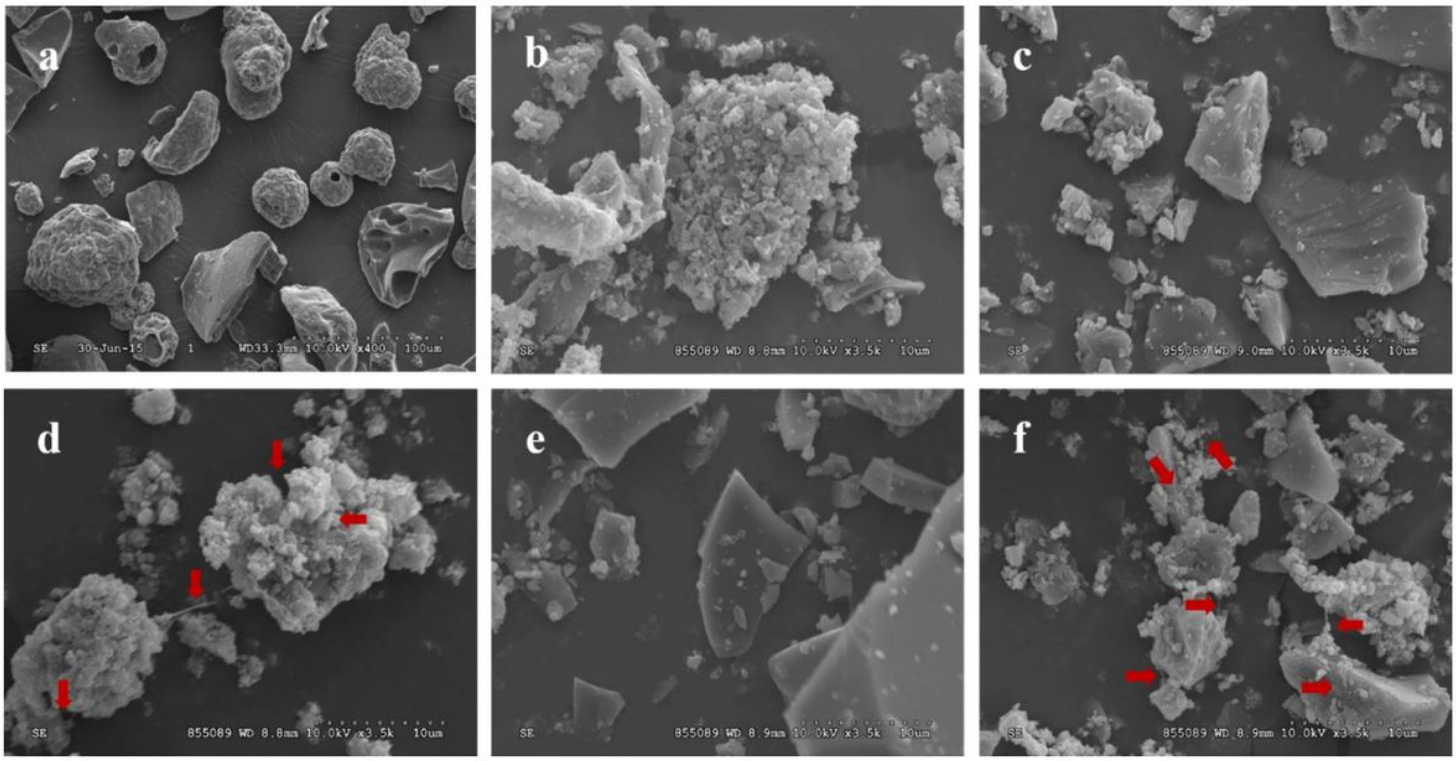

Figure 2

Scanning electron microscope images of lignin: (a) alkaline lignin at 400x magnifications, (b) L4.5, (c) L8.5, (d) L8.5-4.5, (e) L12, and (f) 12-4.5 at 1500x magnifications.

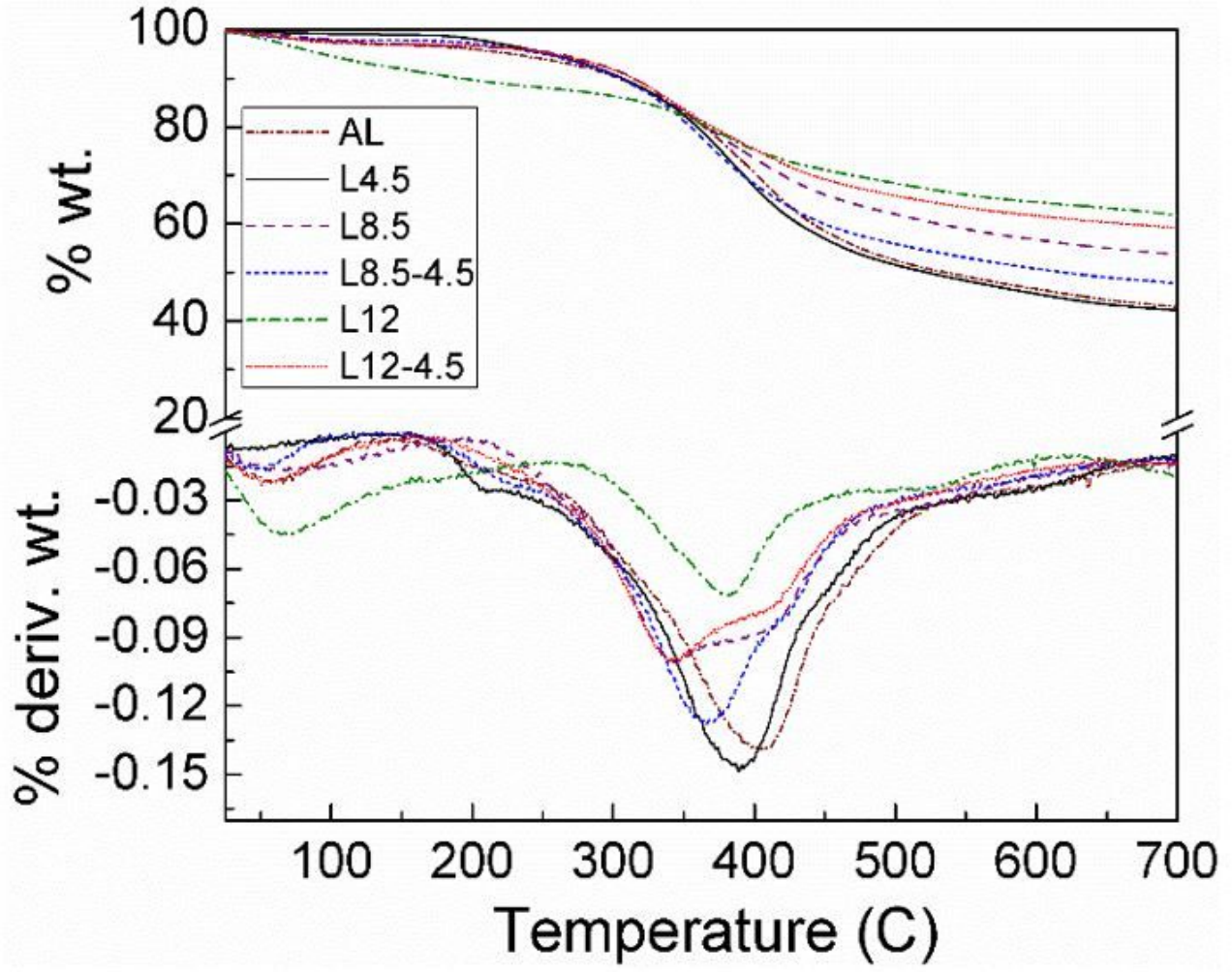

Figure 3

Derivative thermogravimetric curves of lignin treated with different pH values and pH-shifting processes.

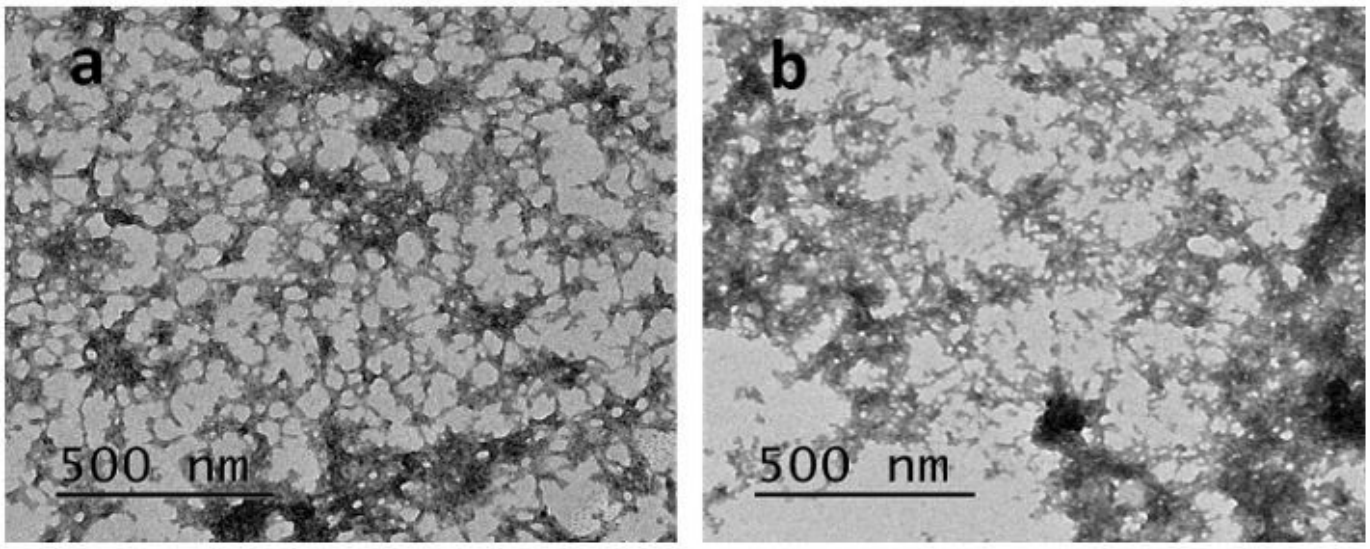

Figure 4

TEM images of (a) SP8.5 and (b) LSP8.5 at 11000x magnifications.

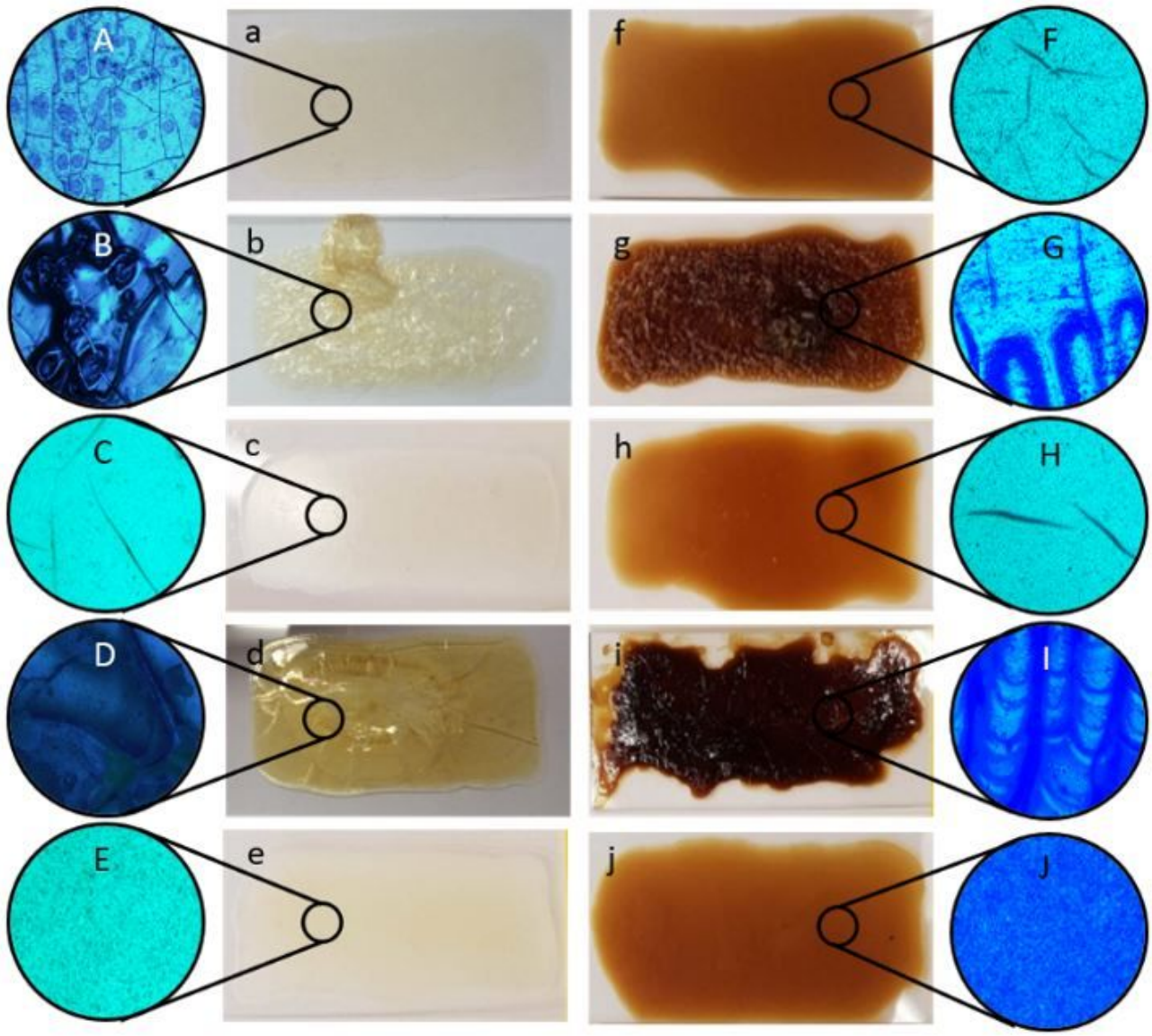

Figure 5

Dried film morphology: (a) SP4.5, (b) SP8.5, (c) SP8.5-4.5, (d) SP12, (e) SP12-4.5, (f) LSP4.5, (g) LSP8.5, (h) LSP8.5-4.5, (i) LSP12, and (j) LSP12-4.5. Optical microscope images of dried film at 5x magnifications: (A) SP4.5, (B) SP8.5, (C) SP8.5-4.5, (D) SP12, (E) SP12-4.5, (F) LSP4.5, (G) LSP8.5, (H) LSP8.5-4.5, (I) LSP12, and (J) LSP12-4.5.

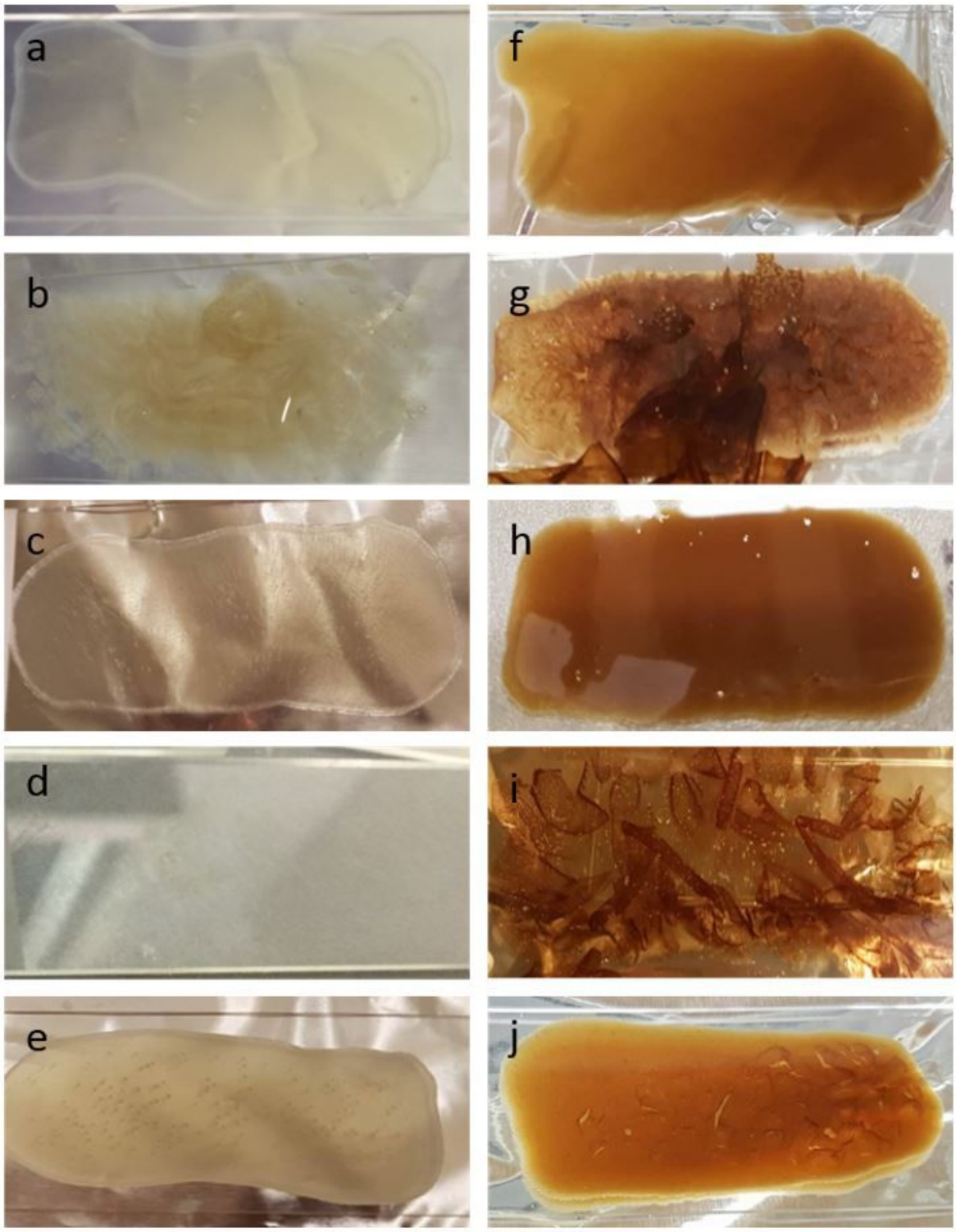

Figure 6

Submerge film morphology: (a) SP4.5, (b) SP8.5, (c) SP8.5-4.5, (d) SP12, (e) SP12-4.5, (f) LSP4.5, (g) LSP8.5, (h) LSP8.5-4.5, (i) LSP12, and (j) LSP12-4.5.

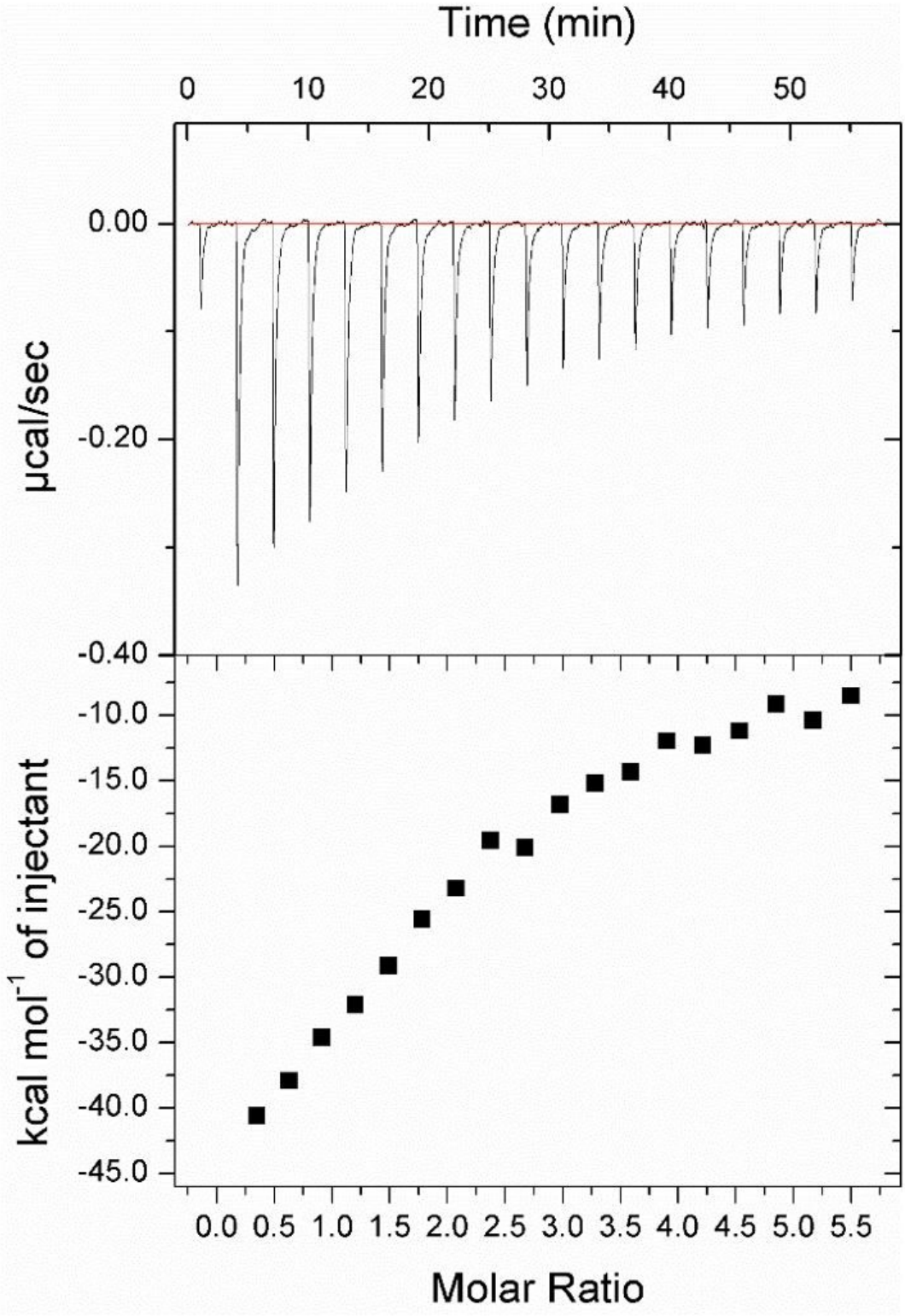

Figure 7

ITC of soy protein with lignin.

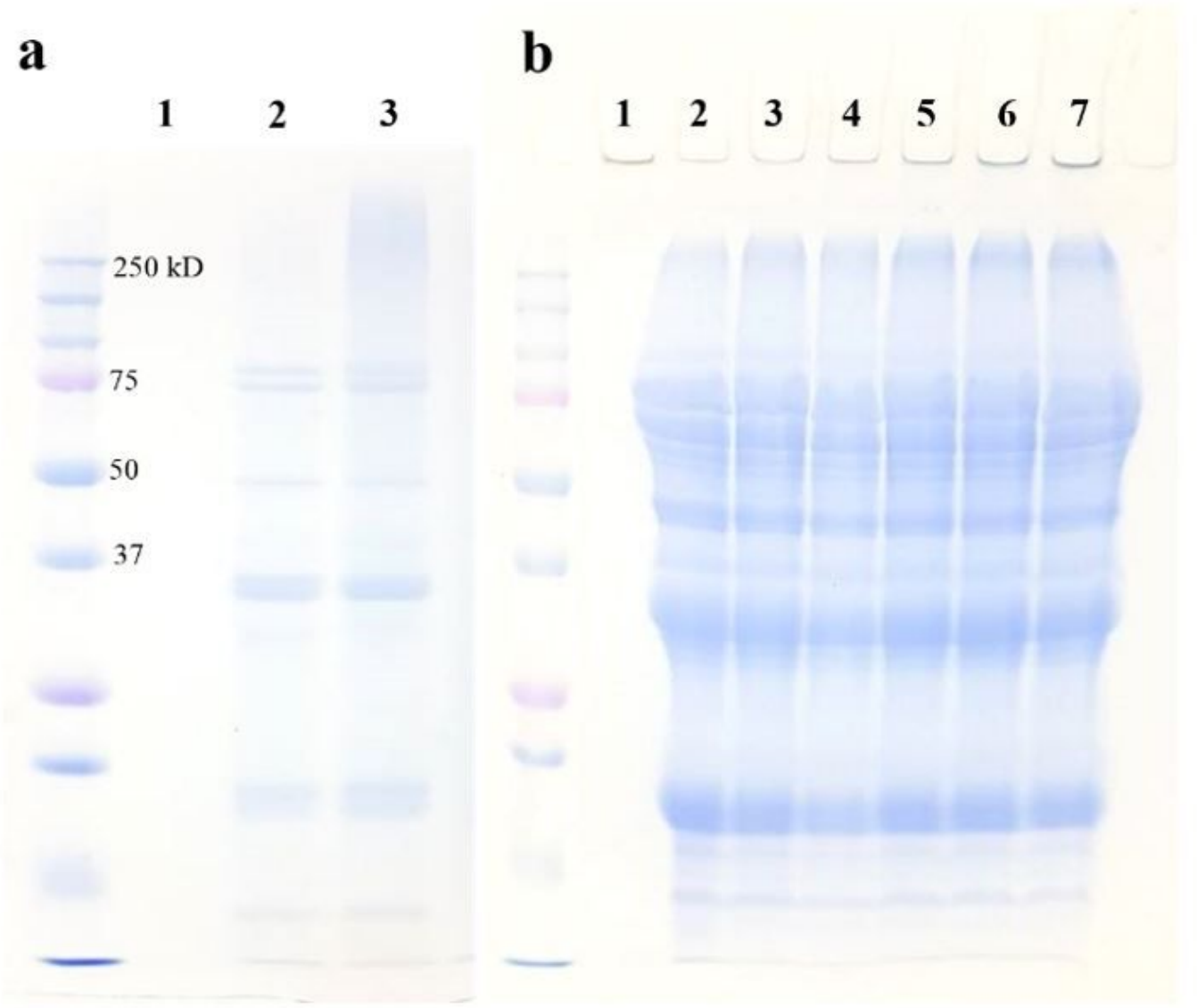

Figure 8

SDS-PAGE patterns at 150 °C. Reducing lignin, SP, and LSP samples: L8.5 (lane 1a), SP8.5 (lane 2a), and LSP8.5 (lane 3a). Fresh samples: L8.5 (lane 1b), SP8.5 (lane 2b), SP+L8.5 (10%) (lane 3b), SP+L8.5 (20%) (lane 4b), SP+L8.5 (30%) (lane 5b), SP+L8.5 (40%) (lane 6b), and SP+L8.5 (50%) (lane 7b).

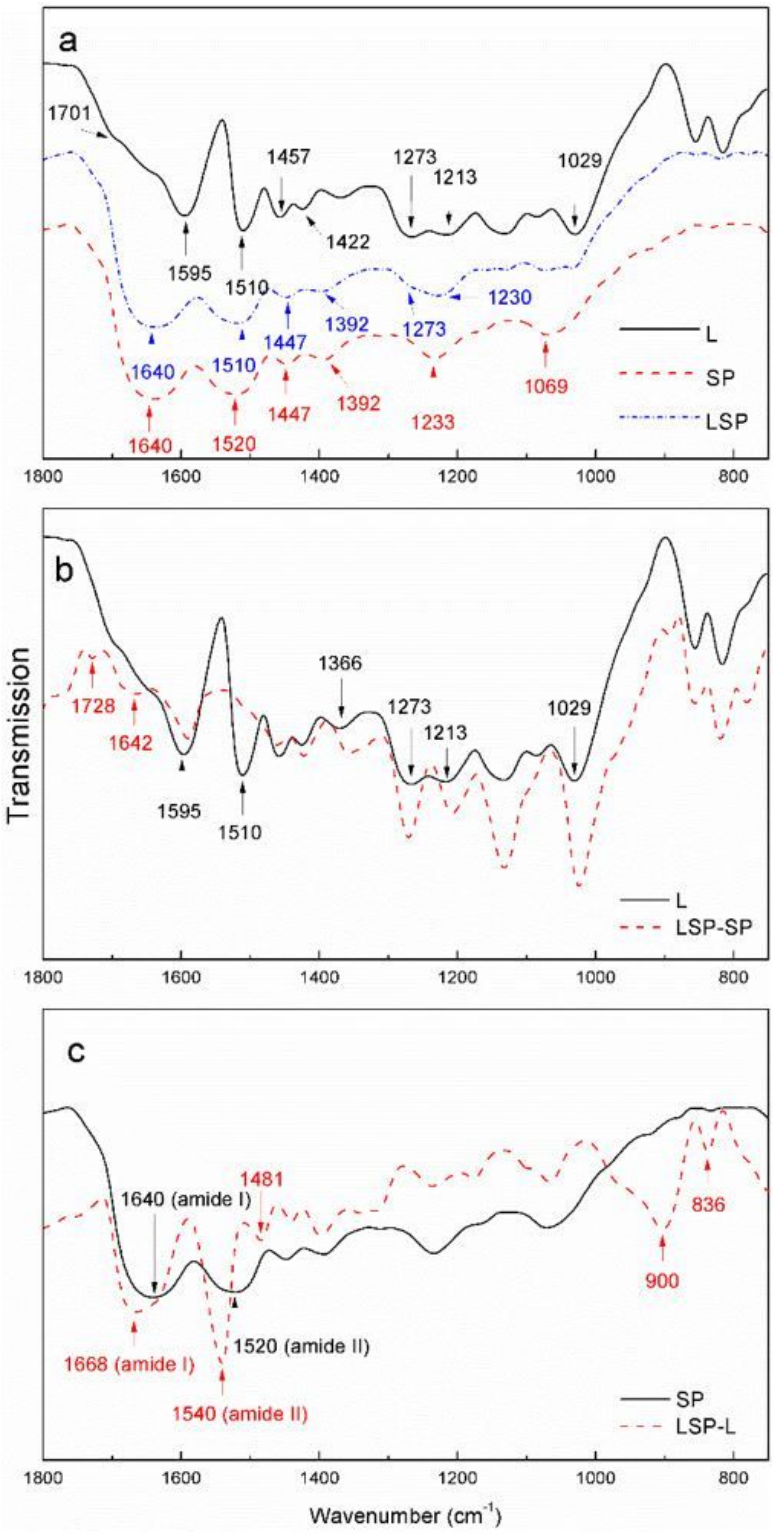

Figure 9

FTIR spectra of lignin, SP, and LSP (a), lignin and subtracted LSP (b), and SP and subtracted LSP (c).